Scientific Research Publishing

Journal of High Energy Physics, Gravitation and Cosmology, 2024, 10, 574-598
https://www.scirp.org/journal/jhepgc
ISSN Online: 2380-4335
ISSN Print: 2380-4327

Classical Cosmology II. The Einstein Ring

Lorenzo Zaninetti

Physics Department, Turin, Italy
Email: l.zaninetti@alice.it

How to cite this paper: Zaninetti, L. (2024) Classical Cosmology II. The Einstein Ring. *Journal of High Energy Physics, Gravitation and Cosmology*, **10**, 574-598.
https://doi.org/10.4236/jhepgc.2024.102036

Received: January 7, 2024
Accepted: March 8, 2024
Published: March 11, 2024

Abstract

The Einstein ring is usually explained in the framework of the gravitational lens. Conversely here we apply the framework of the expansion of a super-bubble (SB) in order to explain the spherical appearance of the ring. Two classical equations of motion for SBs are derived in the presence of a linear and a trigonometric decrease for density. A relativistic equation of motion with an inverse square dependence for the density is derived. The angular distance, adopting the minimax approximation, is derived for three relativistic cosmologies: the standard, the flat and the wCDM. We derive the relation between redshift and Euclidean distance, which allows fixing the radius of the Einstein ring. The details of the ring are explained by a simple version of the theory of images.

Keywords

Cosmology, Observational Cosmology, Gravitational Lenses, Luminous Arcs

1. Introduction

A theoretical prediction of the existence of gravitational lenses (GLs) is due to Einstein in 1936 [1] where the formulae for the optical properties of a gravitational lens for stars A and B were derived. An initial sketch, which dates back to 1912, is reported at p. 585 in [2]. GLs were also predicted by Chwolson in 1924 [3] and therefore before the year 1936: due to this fact, the name Einstein-Chwolson ring appears in the literature. We now report some points of discussion about GLs. An Einstein ring recognition approach based on computer vision techniques was analysed in [4]. A study of the mass discrepancy-acceleration relation (MDAR) of 57 elliptical galaxies by their Einstein rings from the Sloan Lens ACS Survey (SLACS) was carried out in [5]. A collection of GLs has been used as a statistical probe of cosmic shear [6]. An investigation of GLs appears in the context of the MOG modified theory of gravity [7]. Some features of the

Einstein ring are accurately reproduced by allowing a smooth, freely oriented DM halo in the lens model [8]. The line-of-sight shear can be accurately measured from a simple simulated strong lensing image with per cent precision [9]. The historical evolution of a GL can be found in two reviews [10] [11]. When the GL was introduced, super-shells were unknown. Now they are a common field of research in astrophysics. Super-shells started to be observed *firstly* in our galaxy by [12], where 17 expanding H I shells were classified, and *secondly* in external galaxies, see as an example [13], where many super-shells were observed in NGC 1569. In order to model such complex objects, the term super bubble (SB) has been introduced but unfortunately astronomers often associate SBs with sizes of ≈ 10 - 100 pc and super-shells with ring-like structures with sizes of ≈ 1 kpc. At the same time an application of the theory of images explains the limb-brightening visible on the maps of intensity of SBs and allows associating the observed filaments to undetectable SBs, see [14].

The present paper derives the classic equation of motion of an SB for a linear profile of density in the framework of the conservation of energy for the thin layer approximation, see Section 2. A relativistic equation of motion for an SB in the presence of an inverse square profile for the decrease in density is presented in Section 3. Section 4 is devoted to checking the two new equations of motion for the evolution of a supernova remnant (SNR) and a supernova (SN). Section 5 presents an approximation for the angular distance in three relativistic cosmologies: the standard, the flat and the wCDM. Section 6 reviews the existing situation of the Euclidean cosmology. Section 7 presents the results for the Einstein ring and Section 8 reviews the theory of images which allows building a ring.

2. Classic Equation of Motion

The conservation of kinetic energy in spherical coordinates within the framework of the thin layer approximation when thermal effects are negligible is

$$\frac{1}{2}M_0\left(r_0\right)v_0^2=\frac{1}{2}M\left(r\right)v^2, \tag{1}$$

where $M_0\left(r_0\right)$ and $M\left(r\right)$ are the swept masses at r_0 and r, while v_0 and v are the velocities of the thin layer at r_0 and r. The above conservation law, when written as a differential equation, is

$$\frac{1}{2}M\left(r\right)\left(\frac{\mathrm{d}}{\mathrm{d}t}r\left(t\right)\right)^2-\frac{1}{2}M_0v_0^2=0. \tag{2}$$

Different forms of density profiles along the radial direction produce different equations of motion. The already analysed cases for the medium's density are a constant profile, a hyperbolic profile, an inverse square profile, a power law profile, an exponential profile, a Gaussian profile, an auto-gravitating profile and an NFW profile, see [15]. In the two following sections we analyse the linear and the trigonometric decreases in the density of matter.

2.1. Medium with a Linear Profile of Density

We assume that the medium around the SN scales with the piece-wise depen-

dence

$$\rho(r;r_c,b)=\begin{cases}\rho_0 & r<r_0\\ \dfrac{\rho_c(b-r+r_0)}{b} & r_0<r\end{cases}, \tag{3}$$

where ρ_c is the density at $r=0$, r_0 is the radius after which the density starts to decrease and b is an adjustable parameter. The mass swept, M_0, in the interval $[0, r_0]$ is

$$M_0(\rho_c,r_0)=\frac{4}{3}\rho_c\pi r_0^3.$$

The total mass swept, $M(r;r_0,\rho_c)$, in the interval $[0, r]$ is

$$M(r;r_0,\rho_c,b)=\frac{4\rho_c\pi r_0^3}{3}+\frac{\rho_c\pi r^3(-3r+4b+4r_0)}{3b}-\frac{\rho_c\pi r_0^3(r_0+4b)}{3b}. \tag{4}$$

The application of the conservation of energy gives the velocity as a function of the radius:

$$v(r;r_0,b,v_0)=\frac{2\sqrt{b}\,r_0^{\frac{3}{2}}v_0}{\sqrt{4br^3-3r^4+4r^3r_0-r_0^4}}, \tag{5}$$

or

$$\frac{\mathrm{d}}{\mathrm{d}t}r(t)=v(r;r_0,b,v_0). \tag{6}$$

The above ordinary differential equation (ODE) does not have an analytical solution. An approximation for the trajectory is obtained by a series solution of the above ODE to fourth order,

$$\begin{aligned}r(t;r_0,v_0,t_0,b)\approx r_0&+\left(\frac{\sqrt{r_0}\sqrt{b}\,v_0}{\sqrt{r_0b}}-\frac{v_0\left(\sqrt{r_0}\sqrt{b}-\sqrt{r_0b}\right)}{\sqrt{r_0b}}\right)(t-t_0)\\&+\left(\frac{3v_0^2\left(\sqrt{r_0}\sqrt{b}-2\sqrt{r_0b}\right)}{4r_0\sqrt{r_0b}}-\frac{3v_0^2\left(\sqrt{r_0}\sqrt{b}-\sqrt{r_0b}\right)}{4\sqrt{r_0b}\,r_0}\right)(t-t_0)^2\\&+\frac{v_0^3\left(3\sqrt{r_0}\,b^{\frac{3}{2}}+5b\sqrt{r_0b}+2r_0\sqrt{r_0b}\right)(t-t_0)^3}{8\sqrt{r_0b}\,r_0^2b}.\end{aligned} \tag{7}$$

2.2. Medium with a Trigonometric Profile of Density

We assume that the medium around the SN scales with a trigonometric profile of the type

$$\begin{cases}\rho_c & r<r_0\\ \rho_c\cos\left(\dfrac{(r-r_0)\pi}{2b}\right) & r_0<r\end{cases}, \tag{8}$$

where ρ_c is the density at $r=0$, r_0 is the radius after which the density starts to decrease and b is an adjustable parameter. The total mass swept,

$M\left(r;r_0,\rho_c,b\right)$, in the interval [0, r] is

$$M\left(r;r_0,\rho_c,b\right)=\frac{1}{3\pi^2}4\rho_c\left(\pi^3r_0^3+6\pi^2br^2\sin\left(\frac{\left(r-r_0\right)\pi}{2b}\right)+24\pi\cos\left(\frac{\left(r-r_0\right)\pi}{2b}\right)b^2r-24b^2r_0\pi-48b^3\sin\left(\frac{\left(r-r_0\right)\pi}{2b}\right)\right). \tag{9}$$

The velocity as a function of the radius is

$$v\left(r;r_0,b,v_0\right)=\frac{\pi^{\frac{3}{2}}r_0^{\frac{3}{2}}v_0}{D}, \tag{10}$$

where

$$D=\left(\pi^3r_0^3+6\pi^2br^2\sin\left(\frac{\left(r-r_0\right)\pi}{2b}\right)+24\pi\cos\left(\frac{\left(r-r_0\right)\pi}{2b}\right)b^2r-24b^2r_0\pi-48b^3\sin\left(\frac{\left(r-r_0\right)\pi}{2b}\right)\right)^{\frac{1}{2}}. \tag{11}$$

The first order ODE to be solved is

$$\frac{\mathrm{d}}{\mathrm{d}t}r\left(t\right)=\frac{\pi^{\frac{3}{2}}r_0^{\frac{3}{2}}v_0}{D}. \tag{12}$$

A series solution for the above ODE to fourth order is

$$r\left(t;r_0,v_0,t_0,b\right)\approx r_0+\left(\frac{\sqrt{r_0}\sqrt{\pi}v_0}{\sqrt{\pi r_0}}-\frac{v_0\left(\sqrt{r_0}\sqrt{\pi}-\sqrt{\pi r_0}\right)}{\sqrt{\pi r_0}}\right)\left(t-t_0\right)+\left(\frac{3v_0^2\left(\sqrt{r_0}\sqrt{\pi}-2\sqrt{\pi r_0}\right)}{4r_0\sqrt{\pi r_0}}-\frac{3v_0^2\left(\sqrt{r_0}\sqrt{\pi}-\sqrt{\pi r_0}\right)}{4\sqrt{\pi r_0}\,r_0}\right)\left(t-t_0\right)^2+\frac{v_0^3\left(3\sqrt{r_0}\sqrt{\pi}+5\sqrt{\pi r_0}\right)\left(t-t_0\right)^3}{8r_0^2\sqrt{\pi r_0}}. \tag{13}$$

3. Relativistic Equation of Motion

In SR, the total energy of a particle is

$$E=M\gamma c^2, \tag{14}$$

where M is the rest mass, c is the speed of light, γ is the Lorentz factor $\frac{1}{\sqrt{1-\beta^2}}$, $\beta=\frac{v}{c}$ and v is the velocity. The relativistic kinetic energy, E_k, is

$$E_k=Mc^2\left(\gamma-1\right), \tag{15}$$

where the rest energy has been subtracted from the total energy, see formula (23.1) in [16]. The relativistic conservation of kinetic energy in the thin layer approximation in two points $\left(r_0,v_0\right)$ and $\left(r,v\right)$ is

$$M_0\left(r_0\right)c^2\left(\gamma_0-1\right)=M\left(r\right)c^2\left(\gamma-1\right), \tag{16}$$

where $M_0(r_0)$ and $M(r)$ are the swept masses at r_0 and r, respectively, $\gamma_0 = \frac{1}{\sqrt{1-\beta_0^2}}$, v_0 the velocity at r_0 and $\beta_0 = \frac{v_0}{c}$. The already analysed relativistic cases for the medium's density are a constant, a power law profile, an exponential profile and the Emden profile, which is an auto-gravitating profile, see [17]. In the following section we analyse an inverse square profile for the decrease in the density of the matter.

An Inverse Square Profile for the Density

The medium is supposed to scale as

$$\begin{cases} \rho_0 & r < r_0 \\ \frac{\rho_0 r_0^2}{r^2} & r_0 < r \end{cases}, \tag{17}$$

where ρ_c is the density at $r = 0$, and r_0 is the radius after which the density starts to decrease.

The total mass swept, $M(r; r_0, \rho_c)$, in the interval [0, r] is

$$M(r; r_0, \rho_c) = -\frac{8}{3}\rho_c \pi r_0^3 + 4\rho_c r_0^2 \pi r.$$

The conservation of energy in SR gives the following differential equation

$$\frac{\mathrm{d}r(t; r_0, v_0, c)}{\mathrm{d}t} = \frac{PN}{PD}, \tag{18}$$

where

$$PN = \sqrt{r_0}\sqrt{36}\left(\left(\left((r_0 - r)c^2 + v_0^2\left(r - \frac{5r_0}{6}\right)\right)\sqrt{c^2 - v_0^2} + c(c - v_0)(c + v_0)(-r_0 + r)\right)\right.$$
$$\left.\left(\left(\left(\frac{3}{2}r^2 - 3rr_0 + \frac{5}{3}r_0^2\right)c^2 - \frac{3v_0^2(-r_0 + r)^2}{2}\right)\sqrt{c^2 - v_0^2} + cr_0(c - v_0)(c + v_0)(-r_0 + r)\right)\right)^{\frac{1}{2}} c, \tag{19}$$

and

$$PD = 9\sqrt{c^2 - v_0^2}\, c^2 r^2 - 18\sqrt{c^2 - v_0^2}\, c^2 r r_0 + 10\sqrt{c^2 - v_0^2}\, c^2 r_0^2 - 9\sqrt{c^2 - v_0^2}\, r^2 v_0^2$$
$$+ 18\sqrt{c^2 - v_0^2}\, r r_0 v_0^2 - 9\sqrt{c^2 - v_0^2}\, r_0^2 v_0^2 + 6c^3 r r_0 - 6c^3 r_0^2 - 6cr r_0 v_0^2 + 6cr_0^2 v_0^2, \tag{20}$$

which does not have an explicit solution. An implicit solution exists:

$$F(r) - F(r_0) = t - t_0, \tag{21}$$

where

$$F(r) = \frac{FN}{FD}, \tag{22}$$

with

$$FN = \left(2\sqrt{c^2 - v_0^2}\, c r_0 + 3rc^2 - 4r_0 c^2 - 3rv_0^2 + 4r_0 v_0^2\right)$$
$$\times\left(\sqrt{c^2 - v_0^2}\, c r_0 + 3rc^2 - 3r_0 c^2 - 3rv_0^2 + 3r_0 v_0^2\right)$$
$$\times\left(\sqrt{c^2 - v_0^2}\, c r_0 + 6rc^2 - 5r_0 c^2 - 6rv_0^2 + 5r_0 v_0^2\right), \tag{23}$$

and

$$FD = 9\left(c^2 - v_0^2\right)^{\frac{3}{2}} \sqrt{r_0} \left[-54 \left(\frac{\sqrt{c^2 - v_0^2}\, c r_0}{6} + (c - v_0)(c + v_0)\left(r - \frac{5 r_0}{6} \right) \right) \right.$$
$$\times \left(c^2 - \sqrt{c^2 - v_0^2}\, c - v_0^2 \right) \tag{24}$$
$$\left. \times \left(\frac{2 c r_0 \left(-r_0 + r\right) \sqrt{c^2 - v_0^2}}{3} + \left(r^2 - 2 r r_0 + \frac{10}{9} r_0^2 \right) c^2 - v_0^2 \left(-r_0 + r\right)^2 \right) \right]^{\frac{1}{2}} c.$$

4. Astrophysical Tests

We now test the reliability of the numerical and approximate solutions on five SNRs: Tycho, see [18], Cas A, see [19], Cygnus loop, see [20], SN 1006, see [21], and Puppis, see [22] [23] [24].

The three astronomically measurable parameters are the time since the explosion in years, t, the actual observed radius in pc, r, and the present velocity of expansion in km·s^{-1}, see **Table 1**. The astrophysical units are pc for length and yr for time. With these units, the initial velocity is $v_0\left(\mathrm{km \cdot s^{-1}}\right) = 9.7968 \times 10^5 v_0\left(\mathrm{pc \cdot yr^{-1}}\right)$. In all the models here considered, the initial velocity, v_0, is constant in the time interval $\left[0, t_0\right]$.

The goodness of the model is evaluated through the percentage error δ_r of the radius, which is

$$\delta_r = \frac{\left| r_{theo} - r_{obs} \right|}{r_{obs}} \times 100, \tag{25}$$

where r_{obs} is the radius of the SNR as given by the astronomical observations and r_{theo} is the radius suggested by the model. In an analogous way, we can define the percentage error of the velocity. Another useful astrophysical variable is the predicted decrease in the theoretical velocity in 10 years, $\Delta_{10} v\left(\mathrm{km \cdot s^{-1}}\right)$.

4.1. A Classical Test

The numerical results for a medium with a linear decrease in density are presented in **Table 2**. The results for a medium with a cosine profile of density are presented in **Table 3**. **Figure 1** presents the Taylor approximation of the trajectory for the linear profile as given by Equation (7) in the restricted range of time [27.75 yr, 55 yr].

Figure 2 presents the Taylor approximation of the trajectory in the trigonometric profile as given by Equation (13) in the restricted range of time [27.75 yr, 40 yr].

4.2. A Relativistic Test on an SN

In the case of an inverse square profile for the density, we present a numerical solution as given by the numerical integration of the differential Equation (18). **Figure 3** displays the theoretical model for SN 1993J 1993j as well as the observed trajectory [25].

Table 1. Observed astronomical parameters of the SNRs.

Name	Age (yr)	Radius (pc)	Velocity (km·s^{-1})	References
Tycho	442	3.7	5300	Williams *et al.* (2016)
Cas A	328	2.5	4700	Patnaude and Fesen (2009)
Cygnus loop	17000	24.25	250	Chiad *et al.* (2015)
SN 1006	1000	10.19	3100	Uchida *et al.* (2013)
Puppis A	3700	10	3700	Reynoso *et al.* (2017)

Table 2. Theoretical parameters of the SNRs for the equation of motion in the case of conservation of energy with linear decrease in density, see Section 2.1.

Name	t_0 (yr)	r_0 (pc)	$v_0\left(\mathrm{km\cdot s^{-1}}\right)$	b (pc)	$\delta_r(\%)$	$\delta_v(\%)$	$\Delta_{10}v\left(\mathrm{km\cdot s^{-1}}\right)$
Tycho	27.75	0.85	30,000	20	0.064	34.37	−46.66
Cas A	17.3	0.52	30,000	8	0.1	31.78	−55.59
Cygnus loop	50.94	1.55	30,000	50	0.15	140.1	−0.18
SN 1006	88.17	2.7	30,000	100	0.72	36.62	−26.18
Puppis A	35.26	1.08	30,000	100	0.87	44.9	−1.74

Table 3. Theoretical parameters of the SNRs for the equation of motion in the case of conservation of energy with a cosine profile in density, see Section 2.2.

Name	t_0 (yr)	r_0 (pc)	$v_0\left(\mathrm{km\cdot s^{-1}}\right)$	b (pc)	$\delta_r(\%)$	$\delta_v(\%)$	$\Delta_{10}v\left(\mathrm{km\cdot s^{-1}}\right)$
Tycho	28.24	0.86	30,000	12	0.067	34.93	−46.62
Cas A	17.79	0.03	30,000	8	0.863	33.66	−56
Cygnus loop	54.53	1.66	30,000	50	0.28	133.1	−0.18
SN 1006	90.13	2.75	30,000	100	4.58×10^{-4}	36.44	−26.41
Puppis A	35.26	1.08	30,000	100	4.3×10^{-2}	42.27	−1.73

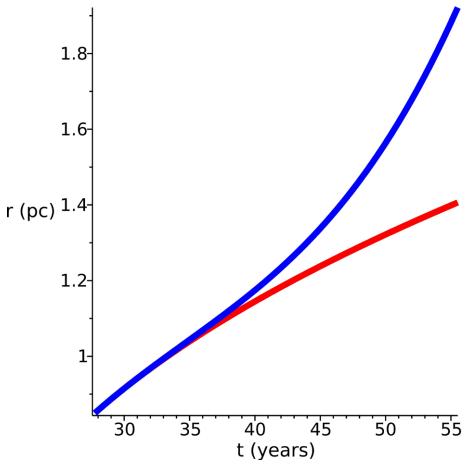

Figure 1. Numerical solution (full red line) and Taylor approximation (blue full line) for the linear profile. Parameters as in **Table 2** for Tycho.

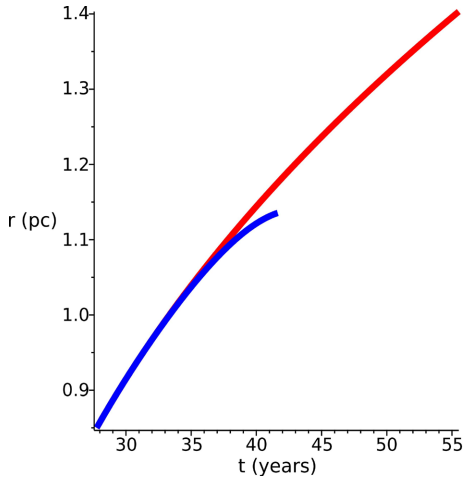

Figure 2. Numerical solution (full red line) and Taylor approximation (blue full line) for the cosine profile. Parameters as in Table 3 for Tycho.

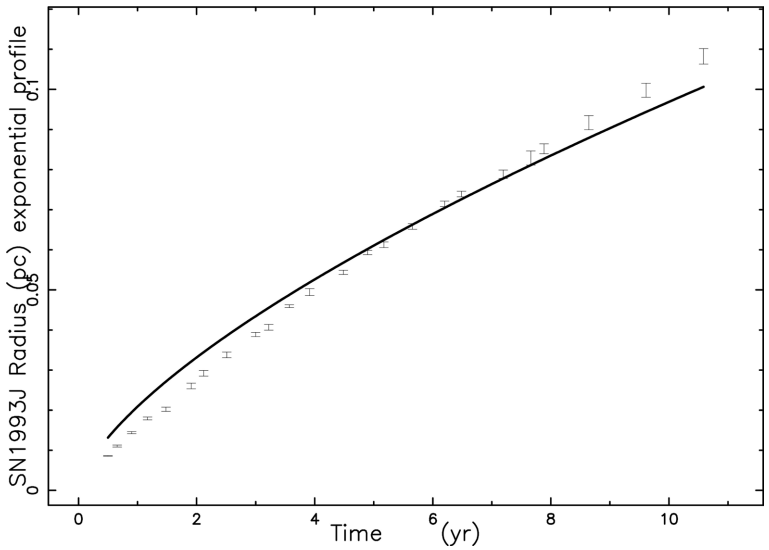

Figure 3. Theoretical radius in the case of an inverse square profile (full line) and astronomical data of SN 1993J 1993j with vertical error bars. The parameters of the model are $r_0 = 5\times10^{-5}$ pc, $t_0 = 1.81\times10^{-4}$ yr and $\beta_0 = 0.9$, which gives $\chi^2 = 5760$.

5. Relativistic Cosmologies

In order to derive the radius in pc of the Einstein ring, we briefly review the angular distance in three relativistic cosmologies: the standard, the flat and the wCDM. The minimax approximation allows the derivation of three approximate formulae for the angular distance which are calibrated on the Pantheon sample [26] [27] [28].

5.1. The Standard Cosmology

In ΛCDM cosmology the *Hubble distance* D_H is defined as

$$D_{\mathrm{H}} \equiv \frac{c}{H_0}, \tag{26}$$

where c is the speed of light and H_0 is the Hubble constant. We then introduce a parameter Ω_{M}

$$\Omega_{\mathrm{M}} = \frac{8\pi G \rho_0}{3H_0^2}, \tag{27}$$

where G is the Newtonian gravitational constant and ρ_0 is the mass density at the present time. Another is Ω_{Λ}

$$\Omega_{\Lambda} \equiv \frac{\Lambda c^2}{3H_0^2}, \tag{28}$$

where Λ is the cosmological constant, see [29]. Once Ω_{Λ} and H_0 are found, the numerical value of the cosmological constant is derived, $\Lambda \approx 1.2 \frac{1}{m^2}$.

The two previous parameters are connected with the curvature Ω_K by

$$\Omega_{\mathrm{M}} + \Omega_{\Lambda} + \Omega_K = 1. \tag{29}$$

The comoving distance, D_{C}, is

$$D_{\mathrm{C}} = D_{\mathrm{H}} \int_0^z \frac{\mathrm{d}z'}{E(z')}, \tag{30}$$

where $E(z)$ is the "Hubble function"

$$E(z) = \sqrt{\Omega_{\mathrm{M}} (1+z)^3 + \Omega_K (1+z)^2 + \Omega_{\Lambda}}. \tag{31}$$

The above integral cannot be done in analytical terms, except for the case of $\Omega_{\Lambda} = 0$, but the Padé approximant, see Appendix A in [28], allows us to derive an approximation for the indefinite integral. In the relativistic models, the angular diameter distance, D_{A} [30], is

$$D_{\mathrm{A}} = \frac{D_{\mathrm{L}}}{(1+z)^2}. \tag{32}$$

We now introduce the minimax approximation. Let $f(x)$ be a real function defined in the interval $[a,b]$. The best rational approximation of degree (k,l) evaluates the coefficients of the ratio of two polynomials of degree k and l, respectively, which minimizes the maximum difference of

$$\max \left| f(x) - \frac{p_0 + p_1 x + \cdots + p_k x^k}{q_0 + q_1 x + \cdots + q_\ell x^\ell} \right|, \tag{33}$$

on the interval $[a,b]$. The quality of the fit is given by the maximum error over the considered range. The coefficients are evaluated through the Remez algorithm, see [31] [32]. The minimax approximation for the angular distance in the interval $0 < z < 8$ with data as in **Table 4** for the ΛCDM cosmology when $k = 2$ and $p = 2$ is

$$D_{A,2,2} = \frac{-0.08214096 + (297.0835166 + 2.721712660z)z}{0.0672226102 + (0.0810609648 + 0.02497466229z)z} \mathrm{Mpc} \tag{34}$$

$$\text{maximum error} = 0.6925458\ \mathrm{Mpc}.$$

Table 4. Numerical values of parameters for the Pantheon sample, H_0 is expressed in km·s^{-1}·Mpc^{-1}; 1048 SN Ia.

Cosmology	Parameters
ΛCDM	$H_0 = 68.209 \pm 0.2$; $\Omega_M = 0.278 \pm 0.02$; $\Omega_\Lambda = 0.651 \pm 0.02$
flat	$H_0 = 69.94 \pm 0.171$; $\Omega_M = 0.296 \pm 0.002$
wCDM	$H_0 = 69.8 \pm 0.27$; $\Omega_M = 0.3 \pm 0.016$; $w = -0.989 \pm 0.03$

A field of investigation in applied cosmology is the maximum of the angular distance as a function of the redshift [33] [34], z_{max}, which is finite in relativistic cosmologies and infinite in Euclidean cosmology. The numerical values of z_{max} are presented in **Table 5**, as a reference $z_{max} = 1.594$ for the flat Planck-ΛCDM cosmology [35].

5.2. The Flat Cosmology

The starting point is Equation (1) for the luminosity distance in [36]

$$D_L(z;c,H_0,\Omega_M) = \frac{c(1+z)}{H_0}\int_0^z \frac{1}{\sqrt{\Omega_M(1+t)^3+1-\Omega_M}}\mathrm{d}t, \tag{35}$$

where the variable of integration, t, denotes the redshift.

By first changing the parameter Ω_M by introducing

$$s = \sqrt[3]{\frac{1-\Omega_M}{\Omega_M}} \tag{36}$$

the luminosity distance becomes

$$D_L(z;c,H_0,s) = \frac{1}{H_0}c(1+z)\int_0^z \frac{1}{\sqrt{\frac{(1+t)^3}{s^3+1}+1-(s^3+1)^{-1}}}\mathrm{d}t. \tag{37}$$

The following change of variable, $t = \frac{s-u}{u}$, is performed for the luminosity distance, which becomes

$$D_L(z;c,H_0,s) = -\frac{c}{H_0 s^2}(1+z)(s^3+1)\int_s^{\frac{s}{1+z}} \frac{u}{u^3+1}\sqrt{\frac{s^3(u^3+1)}{u^3(s^3+1)}}\mathrm{d}u. \tag{38}$$

The integral for the luminosity distance is

$$\begin{aligned} D_L(z;c,H_0,s) = {} & -1/3\frac{c(1+z)3^{3/4}\sqrt{s^3+1}}{\sqrt{s}H_0} \\ & \times\left(F\left(2\frac{\sqrt{s(s+1+z)}\sqrt[4]{3}}{s\sqrt{3}+s+z+1}, 1/4\sqrt{2}\sqrt{3}+1/4\sqrt{2}\right)\right. \\ & \left. -F\left(2\frac{\sqrt[4]{3}\sqrt{s(s+1)}}{s+1+s\sqrt{3}}, 1/4\sqrt{2}\sqrt{3}+1/4\sqrt{2}\right)\right), \end{aligned} \tag{39}$$

Table 5. Numerical values of $z_{\max}$ and radius of Einstein ring in kpc when $R_{\text{ave}} = 1.54$ arcsec.

Cosmology	$z_{\max}$	Radius (kpc)
ΛCDM	1.6403	12.72
flat	1.614	11.88
wCDM	1.591	11.17

where s is given by Equation (36) and $F(\phi,k)$ is Legendre's incomplete elliptic integral of the first kind,

$$F(\phi,k)=\int_0^{\sin\phi}\frac{\mathrm{d}t}{\sqrt{1-t^2}\sqrt{1-k^2t^2}}, \tag{40}$$

see [37]. The minimax approximation for the angular distance in the interval $0<z<8$ with data as in **Table 4** for the flat cosmology when $k=2$ and $p=2$ is

$$D_{A,2,2}=\frac{-0.03784870+(274.0072985+2.188226163z)z}{0.0640891726+(0.0767235768+0.02582989582z)z}\text{Mpc} \tag{41}$$

$$\text{maximum error}=0.629028\ \text{Mpc}.$$

5.3. Dynamical Dark Energy or wCDM

In the dynamical dark energy cosmology (wCDM), first introduced by [38], the *Hubble distance* is

$$D_H(z;\Omega_{\text{M}},w,\Omega_{DE})=\frac{1}{\sqrt{(1+z)^3\,\Omega_{\text{M}}+\Omega_{DE}(1+z)^{3+3w}}}, \tag{42}$$

where w is the equation of state, here considered a constant, see Equation (3.4) in [39] or Equation (18) in [40] for the luminosity distance. Here we assumed w to be constant but the case of w as function of z can also be considered, see Equation (19) in [40]. In the above cosmology the cosmological constant is absent. In flat cosmology

$$\Omega_{\text{M}}+\Omega_{DE}=1, \tag{43}$$

and the *Hubble distance* becomes

$$D_H(z;\Omega_{\text{M}},w)=\frac{1}{\sqrt{(1+z)^3\,\Omega_{\text{M}}+(1-\Omega_{\text{M}})(1+z)^{3+3w}}}. \tag{44}$$

The indefinite integral in the variable z of the above *Hubble distance*, $Iz\equiv\dfrac{D_C}{D_H}$, is

$$Iz(z;\Omega_{\text{M}},w)=\int D_H(z;\Omega_{\text{M}},w)\,\mathrm{d}z, \tag{45}$$

where the new symbol Iz underlines the mathematical operation of integration. In order to find the indefinite integral, we perform a change of variable $1+z=t^{1/3}$

$$Iz\left(t;\Omega_{\mathrm{M}},w\right)=\frac{1}{3}\int\frac{1}{\sqrt{-t\left(\left(-1+\Omega_{\mathrm{M}}\right)t^{w}-\Omega_{\mathrm{M}}\right)}t^{2/3}}\mathrm{d}t. \tag{46}$$

The indefinite integral is

$$Iz\left(t;\Omega_{\mathrm{M}},w\right)=\frac{-2\,{}_2F_1\left(\frac{1}{2},-\frac{1}{6}w^{-1};1-\frac{1}{6}w^{-1};-\frac{t^{w}-\left(1-\Omega_{\mathrm{M}}\right)}{\Omega_{\mathrm{M}}}\right)}{\sqrt{\Omega_{\mathrm{M}}}\sqrt[6]{t}}, \tag{47}$$

where ${}_2F_1\left(a,b;c;z\right)$ is the regularized hypergeometric function, see [37] [41] [42] [43] [44]. We now return to the variable z, the redshift. The indefinite integral becomes

$$Iz\left(z;\Omega_{\mathrm{M}},w\right)=\frac{-2\,{}_2F_1\left(\frac{1}{2},-\frac{1}{6}w^{-1};1-\frac{1}{6}w^{-1};-\frac{\left(-z^3+3z^2+3z+1\right)^{w}\left(1-\Omega_{\mathrm{M}}\right)}{-\Omega_{\mathrm{M}}}\right)}{\sqrt{\Omega_{\mathrm{M}}}\sqrt[6]{z^3+3z^2+3z+1}}. \tag{48}$$

We denote by $F\left(z;\Omega_{\mathrm{M}},w\right)$ the definite integral

$$F\left(z;\Omega_{\mathrm{M}},w\right)=Iz\left(z=z;\Omega_{\mathrm{M}},w\right)-Iz\left(z=0;\Omega_{\mathrm{M}},w\right). \tag{49}$$

The luminosity distance, D_{L}, for the wCDM cosmology in the case of the analytical solution is

$$D_{\mathrm{L}}\left(z;c,H_0,\Omega_{\mathrm{M}},w\right)=\frac{c}{H_0}\left(1+z\right)F\left(z;\Omega_{\mathrm{M}},w\right), \tag{50}$$

where $F\left(z;\Omega_{\mathrm{M}},w\right)$ is given by Equation (49) and the distance modulus is

$$m-M=25+5\log_{10}\left(D_{\mathrm{L}}\left(z;c,H_0,\Omega_{\mathrm{M}},w\right)\right). \tag{51}$$

More details can be found in [45]. The minimax approximation for the angular distance in the interval $0<z<8$ with data as in **Table 4** for the wCDM cosmology when $k=3$ and $p=2$ is

$$D_{A,3,2}=\frac{0.039674109+\left(261.8382247+\left(2.155808744-0.04094111183z\right)z\right)z}{0.0597028175+\left(0.0839556948+0.02480097583z\right)z}\,\mathrm{Mpc} \tag{52}$$

$$\text{maximum error}=0.0622614\,\mathrm{Mpc}.$$

6. Euclidean Cosmology

The New Tired Light (NTL) has equations

$$H_0=\frac{2n_e hr_e}{m_e}, \tag{53a}$$

$$z=\exp\frac{H_0*d}{c}-1 \tag{53b}$$

where n_e is the number density of matter, h is the Planck constant, r_e is the classical radius of the electron, m_e is the mass of the electron, c is the speed of light in km·s^{-1}, d is the distance in Mpc and H_0 is the Hubble constant in km·s^{-1}·Mpc^{-1}; see Equations (13) and (14) in [46]. Inverting the above formula we obtain the distance as a function of the redshift:

$$d = \frac{\ln(z+1)c}{H_0} \text{Mpc}. \tag{54}$$

The transversal distance, d_t in pc, of an astrophysical object in Euclidean cosmology can be obtained from the formula

$$d_t = \frac{4.8481\alpha_{\text{arcsec}} \ln(z+1)c}{H_0} \text{pc}, \tag{55}$$

where α_{arcsec} is the angular distance expressed in arcsec.

7. The Einstein Ring

This section reviews the theory connected with the Einstein ring, the observed lensing system SDP.81, the Canarias ring and the derived numerical results which simulate the ring.

7.1. The Existing Theory

In the case of a circularly symmetric lens and when the source and the length are on the same line of sight, the radius of the ER in radians is

$$\theta_E = \sqrt{\frac{4GM(\theta_E)}{c^2}\frac{D_{ds}}{D_d D_s}}, \tag{56}$$

where $M(\theta_E)$ is the mass enclosed inside the radius of the ER, $D_{d,s,ds}$ are the lens, source and lens-source distances, respectively, G is the Newtonian gravitational constant, and c is the speed of light, see Equation (20) in [47] and Equation (1) in [48]. The mass of the ER can be expressed in units of solar mass, $M_\odot$:

$$M(\theta_{E,\text{arcsec}}) = 1.228\times 10^8 \frac{\Theta^2_{E,\text{arcsec}} D_{ds,\text{Mpc}} D_{s,\text{Mpc}}}{D_{d,\text{Mpc}}} M_\odot, \tag{57}$$

where $\theta_{E,\text{arcsec}}$ is the radius of the ER in arcsec and the three distances are expressed in Mpc.

7.2. The Galaxy-Galaxy Lensing System SDP.81

The ring associated with the galaxy SDP.81, see [49], is generally explained by a GL. In this framework we have a foreground galaxy at $z = 0.2999$ and a background galaxy at $z = 3.042$ [50]. This ring has been studied with the Atacama Large Millimeter/sub-millimeter Array (ALMA) by [50]-[55]. The system SDP.81 as analysed by ALMA presents 14 molecular clumps along the two main lensed arcs. We can therefore speak of the ring's appearance as a "grand design" and we now test the hypothesis of circular symmetry. In order to test the departure from a circle, an observational percentage of reliability is introduced that uses both the size and the shape,

$$\varepsilon_{\text{obs}} = 100\left(1 - \frac{\sum_j \left|R_{\text{obs}} - R_{\text{ave}}\right|_j}{\sum_j R_{\text{obs}\,j}}\right), \tag{58}$$

where R_{obs} is the observed radius in arcsec and R_{ave} is the average radius in arcsec, which is $R_{\text{ave}} = 1.54$ arcsec. Figure 4 presents the astronomical data of SDP.81; the percentage of reliability is $\varepsilon_{\text{obs}} = 92.78\%$. According to Equation (55) the Euclidean average radius of the SDP.81 ring is 46.66 kpc when $c = 299792.458\ \text{km}\cdot\text{s}^{-1}$, $H_0 = 67\ \text{km}\cdot\text{s}^{-1}\cdot\text{Mpc}^{-1}$ and $\alpha_{\text{arcsec}} = 1.54$, see Table 6.

7.3. Canarias ER

The object IAC J010127-334319 has been detected in the optical region with the Gran Telescopio CANARIAS; the background starburst galaxy is at $z = 1.165$ and the radius of the ER is $\theta_E = 2.16$ arcsec according to [48] and $\theta_E = 2.25$ arcsec according to [56]. As an example, inserting the above radius, $D_{s,\text{Mpc}} = 1192$ Mpc, $D_{ls,\text{Mpc}} = 498$ Mpc and $D_{l,\text{Mpc}} = 951$ Mpc in Equation (57), we obtain a mass for the foreground galaxy of $M\left(\theta_{E,\text{arcsec}}\right) = 1.3\times 10^{12} M_{\odot}$. According to Equation (55) the Euclidean average radius of the Canarias ring is 36.19 kpc when $c = 299792.458\ \text{km}\cdot\text{s}^{-1}$, $H_0 = 67\ \text{km}\cdot\text{s}^{-1}\cdot\text{Mpc}^{-1}$ and $\alpha_{\text{arcsec}} = 2.16$, see Table 6.

7.4. Numerical Results

We now simulate the ring connected with SDP.81 and its Euclidean radius of 46.66 kpc. The free parameters of the model with a linear profile are presented in Table 7, Figure 5 presents the law of motion and Figure 6 the behavior of the velocity as a function of time.

The free parameters of the model with a trigonometric profile are presented in Table 8, Figure 7 presents the numerical solution of the law of motion.

The Canarias ring is now simulated in a relativistic framework, see Section 3. The free parameters of the model with an inverse square profile of density are presented in Table 9 and Figure 8 presents the law of motion.

8. The Image

We now briefly review the basic equations of the radiative transfer equation, the conversion of the flux of energy into luminosity and the symmetric theory of the image.

8.1. Radiative Transfer Equation

The transfer equation in the presence of emission and absorption, see for example Equation (1.23) in [57] or Equation (9.4) in [58] or Equation (2.27) in [59], is

$$\frac{\mathrm{d}I_\nu}{\mathrm{d}s} = -k_\nu \zeta I_\nu + j_\nu \zeta, \tag{59}$$

where I_ν is the specific intensity or spectral brightness, s is the line of sight, j_ν the emission coefficient, k_ν a mass absorption coefficient, ζ the mass density at position s, and the index ν denotes the involved frequency of emission. The solution to Equation (59) is

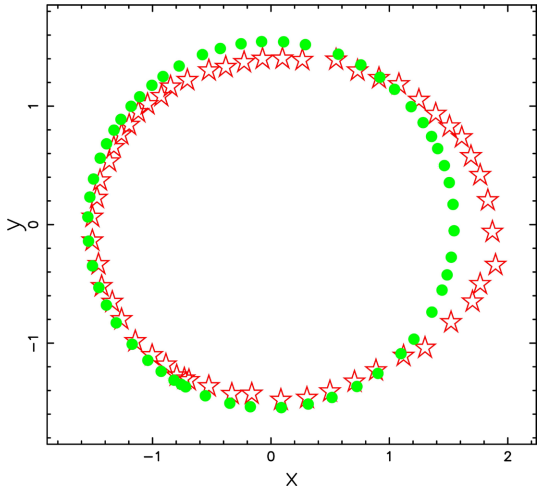

Figure 4. Real data of SDP.81 ring (empty red stars) and average circle (full green points). The real data are extracted by the author from **Figure 6** in [55] using WebPlotDigitizer.

Table 6. Radius of the Einstein ring in kpc for different cosmologies.

Cosmology	SDP.81 ring	Canarias ring
ΛCDM	12.72	18.72
flat	11.88	17.89
wCDM	11.17	16.86
Euclidean	46.66	36.19

Table 7. Theoretical parameters of an SB evolving in a medium with a linear profile.

Name	t (yr)	t_0 (yr)	b (pc)	r_0 (pc)	v_0 (km·s^{-1})
SDP.81	1.5×10^8	32,003	55,992	980	300,000

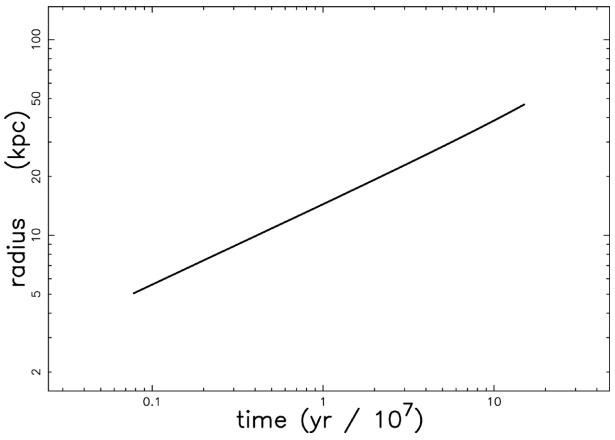

Figure 5. Numerical solution for the radius as function of time for SB associated with SDP.81 (full line) in presence of a linear decrease in density, see Equation (6). Parameters as in **Table 7**, both axes are logarithmic.

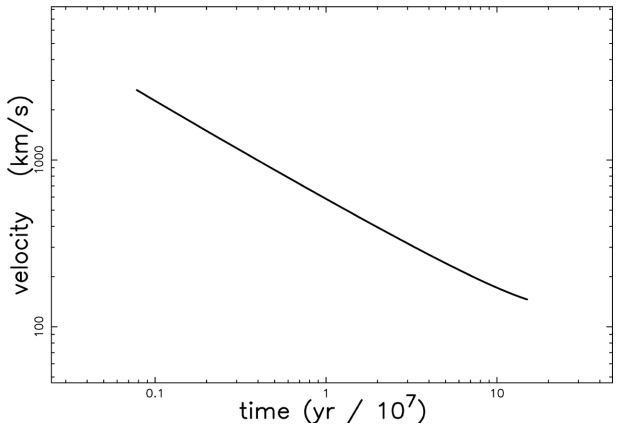

Figure 6. Velocity as a function of time for SDP.81 (full line) in presence of a linear decrease in density. Parameters as in Table 7, both axes are logarithmic.

Table 8. Theoretical parameters of an SB evolving in a medium with a trigonometric profile.

Name	t (yr)	t_0 (yr)	b (pc)	r_0 (pc)	v_0 (km·s^{-1})
SDP.81	2×10^8	32,002	233,300	980	300,000

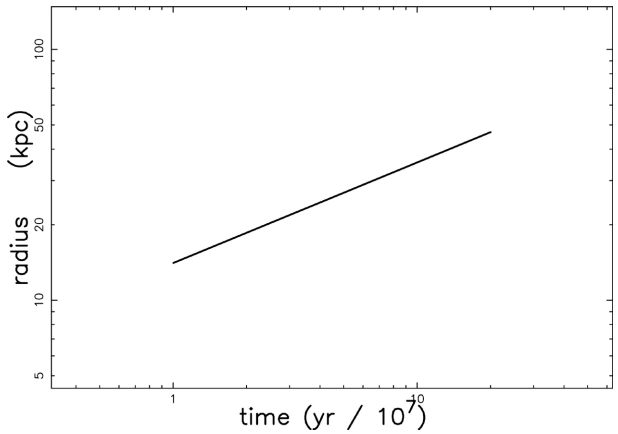

Figure 7. Numerical solution for the radius as function of time for SB associated with SDP.81 (full line) in presence of a trigonometric decrease in density, see ODE (12). Parameters as in Table 8, both axes are logarithmic.

Table 9. Theoretical parameters of a relativistic SB evolving in a medium with an inverse square profile.

Name	t (yr)	t_0 (yr)	r_0 (pc)	β_0
Canarias ring	1.7×10^7	3.26	0.9	0.9

$$I_\nu(\tau_\nu) = \frac{j_\nu}{k_\nu}\left(1 - e^{-\tau_\nu(s)}\right), \tag{60}$$

where τ_ν is the optical depth at frequency ν

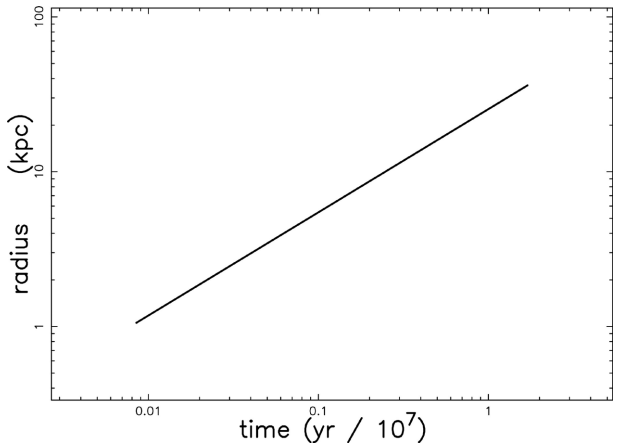

Figure 8. Implicit solution for the relativstic radius as function of time for the SB connected with the Canarias ring (full line) in presence of an inverse square profile for density, see implicit solution (21). Parameters as in **Table 9**, both axes are logarithmic.

$$\mathrm{d}\tau_\nu = k_\nu \zeta \mathrm{d}s. \tag{61}$$

We now continue analysing the case of an optically thin layer in which τ_ν is very small (or k_ν very small) and the density ζ is replaced by the number density of particles, $n(s)$. In the following, the emissivity is taken to be proportional to the number density

$$j_\nu \zeta = Kn(s), \tag{62}$$

where K is a constant. The intensity is therefore

$$I_\nu(s) = I_0 + K\int_{s_0}^{s} n(s')\mathrm{d}s', \tag{63}$$

where I_0 is the intensity at the point s_0. The MKS units of the intensity are $\mathrm{W{\cdot}m^{-2}{\cdot}Hz^{-1}{\cdot}sr^{-1}}$. The increase in brightness is proportional to the number density integrated along the line of sight: in the case of constant number density, it is proportional only to the distance along the line of sight.

As an example, synchrotron emission has an intensity proportional to l, the dimension of the radiating region, in the case of a constant number density of the radiating particles, see formula (1.175) of [60].

8.2. The Source of Luminosity

The ultimate source of the observed luminosity is assumed to be the rate of kinetic energy, L_m,

$$L_m = \frac{1}{2}\rho A V^3, \tag{64}$$

where A is the considered area, V is the velocity of a spherical SB and ρ is the density in the advancing layer of the spherical SB. In the case of the spherical expansion of an SB, $A = 4\pi r^2$, where r is the instantaneous radius of the SB, which means

$$L_m = \frac{1}{2}\rho 4\pi r^2 V^3. \tag{65}$$

The units of the luminosity are W in MKS and erg·s^{-1} in CGS. The astrophysical version of the rate of kinetic energy, L_{ma}, is

$$L_{ma} = 1.39\times 10^{29} n_1 r_1^2 v_1^3 \frac{\text{ergs}}{\text{s}}, \tag{66}$$

where n_1 is the number density expressed in units of 1 particle/cm^3, r_1 is the radius in parsecs, and v_1 is the velocity in km/s. As an example, inserting $r_1 = 46.66\times 10^3$, $n_1 = 0.1$ and $v_1 = 26.08$ in the above formula, the maximum available mechanical luminosity is $L_{ma} = 5.37\times 10^{41}\frac{\text{ergs}}{\text{s}}$. The spectral luminosity, L_ν, at a given frequency ν is

$$L_\nu = 4\pi D_{\text{L}}^2 S_\nu, \tag{67}$$

where S_ν is the observed flux density at the frequency ν with MKS units W·m^{-2}·Hz^{-1}. The observed luminosity at a given frequency ν can be expressed as

$$L_\nu = \varepsilon L_{ma}, \tag{68}$$

where ε is a conversion constant from the mechanical luminosity to the observed luminosity. More details on the synchrotron luminosity and the connected astrophysical units can be found in [59].

8.3. The Theory of a Symmetrical Image

We assume that the number density of the emitting matter n is variable, and in particular rises from 0 at $r = a$ to a maximum value n_m, remains constant up to $r = b$, and then falls again to 0. This geometrical description is shown in **Figure 9**.

The length of the line of sight, when the observer is situated at the infinity of the x-axis, is the locus parallel to the x-axis which crosses the position y in a Cartesian x-y plane and terminates at the external circle of radius b. The length of this locus is

$$\begin{aligned} l_{0a} &= 2\times\left(\sqrt{b^2-y^2}-\sqrt{a^2-y^2}\right);\ 0\le y<a \\ l_{ab} &= 2\times\sqrt{b^2-y^2};\ a\le y<b. \end{aligned} \tag{69}$$

When the number density of the emitting matter n_m is constant between two spheres of radii a and b, the intensity of radiation is

$$\begin{aligned} I_{0a} &= K_I\times n_m\times 2\times\left(\sqrt{b^2-y^2}-\sqrt{a^2-y^2}\right);\ 0\le y<a \\ I_{ab} &= K_I\times n_m\times 2\times\sqrt{b^2-y^2};\ a\le y<b, \end{aligned} \tag{70}$$

where K_I is a constant. The ratio between the theoretical intensity at the maximum ($y = a$) and at the minimum ($y = 0$) is given by

$$\frac{I(y=a)}{I(y=0)} = \frac{\sqrt{b^2-a^2}}{b-a}. \tag{71}$$

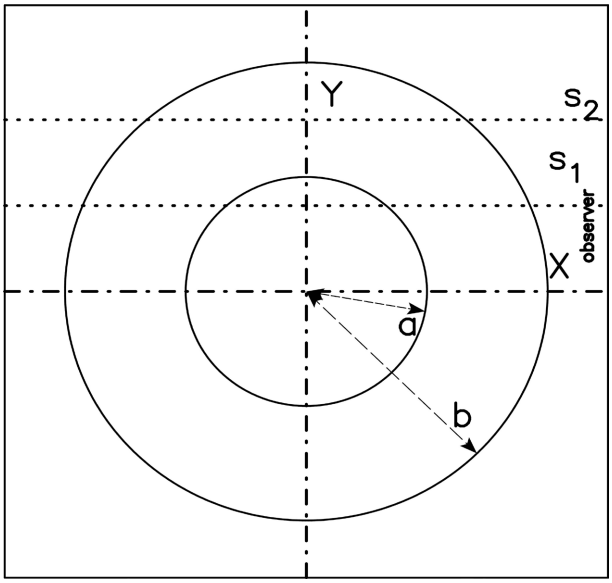

Figure 9. The two circles (sections of spheres) which include the region with constant number density of emitting matter are represented by a full line. The observer is situated along the *x* direction, and three lines of sight are indicated.

The parameter b is identified with the external radius, which means the advancing radius of an SB. The parameter a can be found from the following formula:

$$a=\frac{b\left(\left(\frac{I(y=a)}{I(y=0)}\right)_{\text{obs}}^{2}-1\right)}{\left(\frac{I(y=a)}{I(y=0)}\right)_{\text{obs}}^{2}+1}, \tag{72}$$

where $\left(\frac{I(y=a)}{I(y=0)}\right)_{\text{obs}}$ is the observed ratio between the maximum intensity at the rim and the intensity at the centre. The distance Δy after which the intensity is decreased by a factor f in the region $a \le y < b$ is

$$\Delta y=\frac{2\sqrt{b^2f^2+a^2-b^2}-\sqrt{a^2f^4-b^2f^4+2a^2f^2+2b^2f^2+a^2-b^2}}{2f}. \tag{73}$$

We can now evaluate the half-width half-maximum by analogy with the Gaussian profile $HWHM_U$, which is obtained by the previous formula upon inserting $f=2$:

$$HWHM_U=\frac{1}{2}\sqrt{a^2+3b^2}-\frac{1}{4}\sqrt{25a^2-9b^2}. \tag{74}$$

In the above model, b is associated with the radius of the outer region of the observed ring, a conversely can be deduced from the observed $HWHM_U$:

$$a=\frac{1}{21}\sqrt{441b^2+464HWHM_U^2-32\sqrt{441b^2HWHM_U^2+100HWHM_U^4}}. \tag{75}$$

As an example, inserting in the above formula $b=1.54$ arcsec and $HWHM_U=0.1$ arcsec, we obtain $a=1.46$ arcsec. A cut in the theoretical intensity of SDP.81, see Section 7.2, is presented in Figure 10 and a theoretical image in Figure 11.

The effect of the insertion of a threshold intensity, I_{tr}, which is connected with the observational techniques, is now analysed. The threshold intensity can be parametrized to $I_{\max}$, the maximum value of intensity characterizing the ring: a typical image with a hole is visible in Figure 12 when $I_{tr}=I_{\max}/fac$, where fac is a parameter which allows matching theory with observations.

For a comparison the observed image of the Einstein ring connected with SDP.81 is presented in Figure 13.

9. Conclusions

Equations of motion. We derived two classical equations of motion for an SB by coupling the thin layer approximation with the conservation of energy. The first model implements a profile in the presence of a linear decrease of density and the second a trigonometric profile of density. A relativistic equation of motion for an SB was derived assuming an inverse square profile of density.

Relativistic Cosmologies. The transversal dimension of an astrophysical object is connected in relativistic cosmologies with the angular distance, which is here presented in the framework of the minimax approximation: Equation (34) for the standard cosmology, Equation (41) for the flat cosmology and Equation (52) for the wCDM cosmology. We recall that the angular distance reaches a maximum at $z\approx 1.6$, which produces a big difference from the Euclidean evaluation of the transversal dimension.

Euclidean Cosmology

The transversal distance in the Euclidean cosmology is easily derived, see Equation (55); it scales logarithmicly: $\propto (z+1)$.

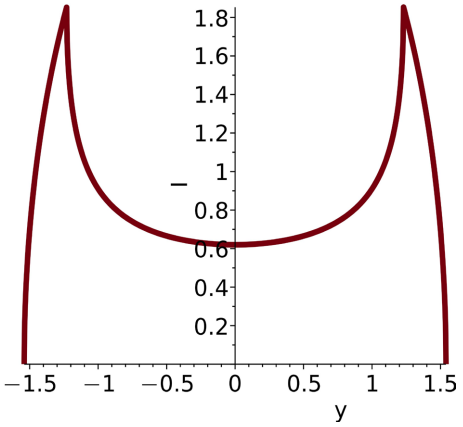

Figure 10. Cut of the intensity I of the ring model, Equation (70), crossing the centre. The x and y axes are in arcsec, $a=1.23$ arcsec, $b=1.54$ arcsec and $\frac{I(y=a)}{I(y=0)}=3$. This cut refers to SDP.81.

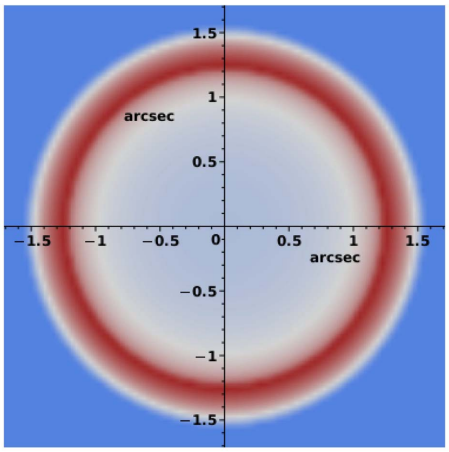

Figure 11. Contour map of I, the x and y axes are in arcsec, parameters as in **Figure 10**.

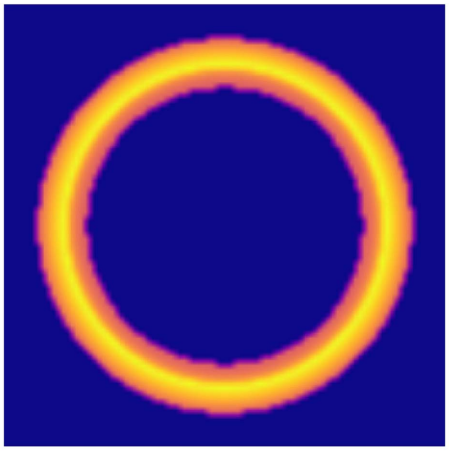

Figure 12. The same as **Figure 11** but with $I_{tr} = I_{\max} / fac$, parameters as in **Figure 10** and $fac = 1.85$.

Figure 13. ALMA image of SDP.81. Credit is given to NRAO/AUI/NSF.

Einstein Ring

Now that a reliable value for the radius of the ER has been derived in the framework of the Euclidean cosmology, we simulate the evolution of the ER in

the framework of the SB. In a classical framework, the results for the radius versus time are presented in Figure 5 for a linear decrease in the surrounding density and in Figure 7 for a trigonometric decrease in density. In a relativistic framework the temporal evolution in the presence of an inverse square profile for the Canarias ring is presented in Figure 8. A geometrical model based on the length of the line of sight allows the appearance of the image, see Figure 12.

Conflicts of Interest

The author declares no conflicts of interest regarding the publication of this paper.

References

[1] Einstein, A. (1936) Lens-Like Action of a Star by the Deviation of Light in the Gravitational Field. *Science*, **84**, 506-507. https://doi.org/10.1126/science.84.2188.506

[2] Einstein, A. (1994) The Collected Papers of Albert Einstein, Volume 3: The Swiss Years: Writings, 1909-1911. Princeton University Press, Princeton.

[3] Chwolson, O. (1924) ÜBer Eine Mögliche Form Fiktiver Doppelsterne. *Astronomische Nachrichten*, **221**, 329-330. https://doi.org/10.1002/asna.19242212003

[4] Lee, C.H. (2017) A Computer Vision Approach to Identify Einstein Rings and Arcs. *Publications of the Astronomical Society of Australia*, **34**, e014. https://doi.org/10.1017/pasa.2017.7

[5] Tian, Y. and Ko, C.M. (2017) Mass Discrepancy—Acceleration Relation in Einstein Rings. *Monthly Notices of the Royal Astronomical Society*, **472**, 765-771. https://doi.org/10.1093/mnras/stx2056

[6] Birrer, S., Refregier, A. and Amara, A. (2018) Cosmic Shear with Einstein Rings. *The Astrophysical Journal Letters*, **852**, L14. https://doi.org/10.3847/2041-8213/aaa1de

[7] Moffat, J., Rahvar, S. and Toth, V. (2018) Applying MOG to Lensing: Einstein Rings, Abell 520 and the Bullet Cluster. *Galaxies*, **6**, Article 43. https://doi.org/10.3390/galaxies6020043

[8] Chen, M.C., Broadhurst, T., Lim, J., Molnar, S.M., Diego, J.M., Oguri, M. and Lee, L.L. (2020) Geometric Support for Dark Matter by an Unaligned Einstein Ring in A3827. *The Astrophysical Journal*, **898**, Article No. 81. https://doi.org/10.3847/1538-4357/ab9ebc

[9] Hogg, N.B., Fleury, P., Larena, J. and Martinelli, M. (2023) Measuring Line-of-Sight Shear with Einstein Rings: A Proof of Concept. *Monthly Notices of the Royal Astronomical Society*, **520**, 5982-6000. https://doi.org/10.1093/mnras/stad512

[10] Valls-Gabaud, D. (2006) The Conceptual Origins of Gravitational Lensing. *Albert Einstein Century International Conference*, Paris, 18-22 July 2005, 1163. https://doi.org/10.1063/1.2399715

[11] Meneghetti, M. (2021) A Brief History of Gravitational Lensing. In: Meneghetti, M., Ed., *Introduction to Gravitational Lensing*, Springer, Cham, 3-19. https://doi.org/10.1007/978-3-030-73582-1_1

[12] Heiles, C. (1979) H I Shells and Supershells. *The Astrophysical Journal*, **229**, 533-537, 539-544. https://doi.org/10.1086/156986

[13] Sánchez-Cruces, M., Rosado, M., Rodrguez-González, A. and Reyes-Iturbide, J.

(2015) Kinematics of Superbubbles and Supershells in the Irregular Galaxy, NGC 1569. *The Astrophysical Journal*, **799**, Article 231. https://doi.org/10.1088/0004-637X/799/2/231

[14] Zaninetti, L. (2012) Evolution of Superbubbles in a Self-Gravitating Disc. *Monthly Notices of the Royal Astronomical Society*, **425**, 2343-2351. https://doi.org/10.1111/j.1365-2966.2012.21649.x

[15] Zaninetti, L. (2020) Energy Conservation in the Thin Layer Approximation: I. The Spherical Classic Case for Supernovae Remnants. *International Journal of Astronomy and Astrophysics*, **10**, 71-88. https://doi.org/10.4236/ijaa.2020.102006

[16] Freund, J. (2008) Special Relativity for Beginners: A Textbook for Undergraduates. World Scientific Press, Singapore. https://doi.org/10.1142/6601

[17] Zaninetti, L. (2020) Energy Conservation in the Thin Layer Approximation: III. The Spherical Relativistic Case for Supernovae. *International Journal of Astronomy and Astrophysics*, **10**, 285-301. https://doi.org/10.4236/ijaa.2020.104015

[18] Williams, B.J., Chomiuk, L., Hewitt, J.W., Blondin, J.M., Borkowski, K.J., Ghavamian, P., Petre, R. and Reynolds, S.P. (2016) An X-Ray and Radio Study of the Varying Expansion Velocities in Tycho Supernova Remnant. *The Astrophysical Journal Letters*, **823**, L32. https://doi.org/10.3847/2041-8205/823/2/L32

[19] Patnaude, D.J. and Fesen, R.A. (2009) Proper Motions and Brightness Variations of Nonthermal X-Ray Filaments in the Cassiopeia a Supernova Remnant. *The Astrophysical Journal*, **697**, 535-543. https://doi.org/10.1088/0004-637X/697/1/535

[20] Chiad, B.T., Ali, L.T. and Hassani, A.S. (2015) Determination of Velocity and Radius of Supernova Remnant after 1000 Yrs of Explosion. *International Journal of Astronomy and Astrophysics*, **5**, 125-132. https://doi.org/10.4236/ijaa.2015.52016

[21] Uchida, H., Yamaguchi, H. and Koyama, K. (2013) Asymmetric Ejecta Distribution in SN 1006. *The Astrophysical Journal*, **771**, Article 56. https://doi.org/10.1088/0004-637X/771/1/56

[22] Winkler, P.F., Tuttle, J.H., Kirshner, R.P. and Irwin, M.J. (1988) Kinematics of Oxygen-Rich Filaments in Puppis A. *International Astronomical Union Colloquium*, **101**, 65-68. https://doi.org/10.1017/S0252921100102131

[23] Aschenbach, B. (2015) Age and Distance of Puppis A Revised—The Supernova Remnant of the 'Star of Bethlehem'. *Proceedings Frascati Workshop* 2015 *on Multifrequency Behaviour of High Energy Cosmic Sources—XI* (*MULTIF*15), Palermo, 25-30 May 2015, 21. https://doi.org/10.22323/1.246.0021

[24] Reynoso, E.M., Cichowolski, S. and Walsh, A.J. (2017) A High-Resolution H I Study towards the Supernova Remnant Puppis A and Its Environments. *Monthly Notices of the Royal Astronomical Society*, **464**, 3029-3039. https://doi.org/10.1093/mnras/stw2219

[25] Marcaide, J.M., Mart-Vidal, I., Alberdi, A. and Pérez-Torres, M.A. (2009) A Decade of SN 1993J: Discovery of Radio Wavelength Effects in the Expansion Rate. *Astronomy & Astrophysics*, **505**, 927-945. https://doi.org/10.1051/0004-6361/200912133

[26] Jones, D.O., Scolnic, D.M., Riess, A.G., *et al.* (2018) Measuring Dark Energy Properties with Photometrically Classified Pan-STARRS Supernovae. II. Cosmological Parameters. *The Astrophysical Journal*, **857**, Article 51. https://doi.org/10.3847/1538-4357/aab6b1

[27] Scolnic, D.M., Jones, D.O., Rest, A., *et al.* (2018) The Complete Light-Curve Sample of Spectroscopically Confirmed SNe Ia from Pan-STARRS1 and Cosmological Constraints from the Combined Pantheon Sample. *The Astrophysical Journal*, **859**, Ar-

ticle 101. https://doi.org/10.3847/1538-4357/aab9bb

[28] Zaninetti, L. (2021) Sparse Formulae for the Distance Modulus in Cosmology. *Journal of High Energy Physics, Gravitation and Cosmology*, **7**, 965-992. https://doi.org/10.4236/jhepgc.2021.73057

[29] Peebles, P.J.E. (1993) Principles of Physical Cosmology. Princeton University Press, Princeton.

[30] Etherington, I.M.H. (1933) On the Definition of Distance in General Relativity. *Philosophical Magazine*, **15**, 761-775. https://doi.org/10.1080/14786443309462220

[31] Remez, E. (1934) Sur la détermination des polynômes d'approximation de degré donnée. *Communions Societatis Mathematicae Kharkovensis*, **10**, 41.

[32] Remez, E. (1957) General Computation Methods of Chebyshev Approximation. The Problems with Linear Real Parameters. Publishing House of the Academy of Science of the Ukrainian SSR, Kiev.

[33] Braatz, J.A., Reid, M.J., Humphreys, E.M.L., Henkel, C., Condon, J.J. and Lo, K.Y. (2010) The Megamaser Cosmology Project. II. The Angular-Diameter Distance to UGC 3789. *The Astrophysical Journal*, **718**, Article 657. https://doi.org/10.1088/0004-637X/718/2/657

[34] Kuo, C.Y., Braatz, J.A., Reid, M.J., Lo, K.Y., Condon, J.J., Impellizzeri, C.M.V. and Henkel, C. (2013) The Megamaser Cosmology Project. V. An Angular-Diameter Distance to NGC 6264 at 140 Mpc. *The Astrophysical Journal*, **767**, Article 155. https://doi.org/10.1088/0004-637X/767/2/155

[35] Melia, F. and Yennapureddy, M.K. (2018) The Maximum Angular-Diameter Distance in Cosmology. *Monthly Notices of the Royal Astronomical Society*, **480**, 2144-2152. https://doi.org/10.1093/mnras/sty1962

[36] Baes, M., Camps, P. and Van De Putte, D. (2017) Analytical Expressions and Numerical Evaluation of the Luminosity Distance in a Flat Cosmology. *Monthly Notices of the Royal Astronomical Society*, **468**, 927-930. https://doi.org/10.1093/mnras/stx537

[37] Olver, F.W.J., Lozier, D.W., Boisvert, R.F. and Clark, C.W. (2010) NIST Handbook of Mathematical Functions, Cambridge University Press, Cambridge.

[38] Turner, M.S. and White, M. (1997) CDM Models with a Smooth Component. *Physical Review D*, **56**, R4439. https://doi.org/10.1103/PhysRevD.56.R4439

[39] Tripathi, A., Sangwan, A. and Jassal, H.K. (2017) Dark Energy Equation of State Parameter and Its Evolution at Low Redshift. *Journal of Cosmology and Astroparticle Physic*, **6**, 012. https://doi.org/10.1088/1475-7516/2017/06/012

[40] Wei, J.J., Ma, Q.B. and Wu, X.F. (2015) Utilizing the Updated Gamma-Ray Bursts and Type Ia Supernovae to Constrain the Cardassian Expansion Model and Dark Energy. *Advances in Astronomy*, **2015**, Article ID: 576093. https://doi.org/10.1155/2015/576093

[41] Abramowitz, M. and Stegun, I.A. (1965) Handbook of Mathematical Functions with Formulas, Graphs, and Mathematical Tables. Dover, New York. https://doi.org/10.1063/1.3047921

[42] Von Seggern, D. (1992) CRC Standard Curves and Surfaces. CRC Press, New York.

[43] Thompson, W.J. (1997) Atlas for Computing Mathematical Functions. Wiley-Interscience, New York.

[44] Gradshteyn, I.S., Ryzhik, I.M., Jeffrey, A. and Zwillinger, D. (2007) Table of Integrals, Series, and Products. Academic Press, New York.

[45] Zaninetti, L. (2019) The Distance Modulus in Dark Energy and Cardassian Cos-

mologies via the Hypergeometric Function. *International Journal of Astronomy and Astrophysics*, **9**, 231-246. https://doi.org/10.4236/ijaa.2019.93017

[46] Ashmore, L.E. (2022) Data from 14,577 Cosmological Objects and 14 FRBs Confirm the Predictions of New Tired Light (NTL) and Lead to a New Model of the IGM. *Journal of Physics*: *Conference Series*, **2197**, Article ID: 012003. https://doi.org/10.1088/1742-6596/2197/1/012003

[47] Narayan, R. and Bartelmann, M. (1996) Lectures on Gravitational Lensing. arXiv: astro-ph/9606001.

[48] Bettinelli, M., Simioni, M., Aparicio, A., Hidalgo, S.L., Cassisi, S., Walker, A.R., Piotto, G. and Valdes, F. (2016) The Canarias Einstein Ring: A Newly Discovered Optical Einstein Ring. *Monthly Notices of the Royal Astronomical Society*: *Letters*, **461**, L67-L71. https://doi.org/10.1093/mnrasl/slw097

[49] Eales, S., Dunne, L., Clements, D. and Cooray, A. (2010) The Herschel ATLAS. *Publications of the Astronomical Society of the Pacific*, **122**, 499.

[50] ALMA Partnership, Vlahakis, C., Hunter, T.R. and Hodge, J.A. (2015) The 2014 ALMA Long Baseline Campaign: Observations of the Strongly Lensed Submillimeter Galaxy HATLAS J090311.6+003906 at $z = 3.042$. *The Astrophysical Journal Letters*, **808**, L4. https://doi.org/10.1088/2041-8205/808/1/L4

[51] Tamura, Y., Oguri, M., Iono, D., Hatsukade, B., Matsuda, Y. and Hayashi, M. (2015) High-Resolution ALMA Observations of SDP.81. I. The Innermost Mass Profile of the Lensing Elliptical Galaxy Probed by 30 Milli-Arcsecond Images. *Publications of the Astronomical Society of Japan*, **67**, 72. https://doi.org/10.1093/pasj/psv040

[52] Rybak, M., Vegetti, S., McKean, J.P., Andreani, P. and White, S.D.M. (2015) ALMA Imaging of SDP.81—II. A Pixelated Reconstruction of the CO Emission Lines. *Monthly Notices of the Royal Astronomical Society*: *Letters*, **453**, L26-L30. https://doi.org/10.1093/mnrasl/slv092

[53] Hatsukade, B., Tamura, Y., Iono, D., Matsuda, Y., Hayashi, M. and Oguri, M. (2015) High-Resolution ALMA Observations of SDP.81. II. Molecular Clump Properties of a Lensed Submillimeter Galaxy at $z = 3.042$. *Publications of the Astronomical Society of Japan*, **67**, 93. https://doi.org/10.1093/pasj/psv061

[54] Wong, K.C., Suyu, S.H. and Matsushita, S. (2015) The Innermost Mass Distribution of the Gravitational Lens SDP.81 from ALMA Observations. *The Astrophysical Journal*, **811**, Article 115. https://doi.org/10.1088/0004-637X/811/2/115

[55] Hezaveh, Y.D., Dalal, N. and Marrone, D.P. (2016) Detection of Lensing Substructure Using ALMA Observations of the Dusty Galaxy SDP.81. *The Astrophysical Journal*, **823**, Article 37. https://doi.org/10.3847/0004-637X/823/1/37

[56] Lee, C.H. (2016) A Closer Look at the Canarias Einstein Ring. *Monthly Notices of the Royal Astronomical Society*, **462**, 3006-3010. https://doi.org/10.1093/mnras/stw1885

[57] Rybicki, G. and Lightman, A. (1991) Radiative Processes in Astrophysics. Wiley-Interscience, New York.

[58] Hjellming, R.M. (1988) Radio Stars in Galactic and Extragalactic Radio Astronomy. Springer-Verlag, Berlin. https://doi.org/10.1007/978-1-4612-3936-9_9

[59] Condon, J.J. and Ransom, S.M. (2016) Essential Radio Astronomy. Princeton University Press, Princeton. https://doi.org/10.1515/9781400881161

[60] Lang, K.R. (1999) Astrophysical Formulae. 3rd Edition, Springer-Verlag, Berlin.